

Article

In-Season Monitoring of Maize Leaf Water Content Using Ground-Based and UAV-Based Hyperspectral Data

Luís Guilherme Teixeira Crusiol^{1,2}, Liang Sun^{1,*} , Zheng Sun¹, Ruiqing Chen¹, Yongfeng Wu³, Juncheng Ma³ and Chenxi Song³

- ¹ Key Laboratory of Agricultural Remote Sensing, Ministry of Agriculture and Rural Affairs/CAAS-CIAT Joint Laboratory in Advanced Technologies for Sustainable Agriculture—Institute of Agricultural Resources and Regional Planning, Chinese Academy of Agricultural Sciences, Beijing 100081, China; luiscrusiol@gmail.com (L.G.T.C.); 82101201128@caas.cn (Z.S.); chenrq@mails.ccau.edu.cn (R.C.)
- ² Embrapa Soja (National Soybean Research Center—Brazilian Agricultural Research Corporation), Londrina 86001-970, PR, Brazil
- ³ Institute of Environment and Sustainable Development in Agriculture, Chinese Academy of Agricultural Sciences, Beijing 100081, China; wuyongfeng@caas.cn (Y.W.); majuncheng@caas.cn (J.M.); 201910852072@ecut.edu.cn (C.S.)
- * Correspondence: sunliang@caas.cn

Abstract: China is one the largest maize (*Zea mays* L.) producer worldwide. Considering water deficit as one of the most important limiting factors for crop yield stability, remote sensing technology has been successfully used to monitor water relations in the soil–plant–atmosphere system through canopy and leaf reflectance, contributing to the better management of water under precision agriculture practices and the quantification of dynamic traits. This research was aimed to evaluate the relation between maize leaf water content (LWC) and ground-based and unoccupied aerial vehicle (UAV)-based hyperspectral data using the following approaches: (I) single wavelengths, (II) broadband reflectance and vegetation indices, (III) optimum hyperspectral vegetation indices (HVIs), and (IV) partial least squares regression (PLSR). A field experiment was undertaken at the Chinese Academy of Agricultural Sciences, Beijing, China, during the 2020 cropping season following a split plot model in a randomized complete block design with three blocks. Three maize varieties were subjected to three differential irrigation schedules. Leaf-based reflectance (400–2500 nm) was measured with a FieldSpec 4 spectroradiometer, and canopy-based reflectance (400–1000 nm) was collected with a Pika-L hyperspectral camera mounted on a UAV at three assessment days. Both sensors demonstrated similar shapes in the spectral response from the leaves and canopy, with differences in reflectance intensity across near-infrared wavelengths. Ground-based hyperspectral data outperformed UAV-based data for LWC monitoring, especially when using the full spectra (Vis–NIR–SWIR). The HVI and the PLSR models were demonstrated to be more suitable for LWC monitoring, with a higher HVI accuracy. The optimal band combinations for HVI were centered between 628 and 824 nm (R^2 from 0.28 to 0.49) using the UAV-based sensor and were consistently located around 1431–1464 nm and 2115–2331 nm (R^2 from 0.59 to 0.80) using the ground-based sensor on the three assessment days. The obtained results indicate the potential for the complementary use of ground-based and UAV-based hyperspectral data for maize LWC monitoring.

Keywords: *Zea mays* L.; leaf reflectance; canopy reflectance; hyperspectral vegetation index; partial least squares regression



Citation: Crusiol, L.G.T.; Sun, L.; Sun, Z.; Chen, R.; Wu, Y.; Ma, J.; Song, C. In-Season Monitoring of Maize Leaf Water Content Using Ground-Based and UAV-Based Hyperspectral Data. *Sustainability* **2022**, *14*, 9039. <https://doi.org/10.3390/su14159039>

Academic Editors: Carlos Antonio Da Silva Junior and Paulo Eduardo Teodoro

Received: 21 June 2022

Accepted: 21 July 2022

Published: 23 July 2022

Publisher's Note: MDPI stays neutral with regard to jurisdictional claims in published maps and institutional affiliations.



Copyright: © 2022 by the authors. Licensee MDPI, Basel, Switzerland. This article is an open access article distributed under the terms and conditions of the Creative Commons Attribution (CC BY) license (<https://creativecommons.org/licenses/by/4.0/>).

1. Introduction

Maize (*Zea mays* L.) plays an important role in world food production and the grain market, and its monitoring is crucial to subsidize economic policies and food security strategies. Worldwide, about 200 million ha are expected to be sown with maize in the 2021/2022 cropping season, with an expected production of over 1000 Mt [1]. China

accounts for over 42 million ha of maize crop and is responsible for over 21% (268 Mt) of all maize produced worldwide, delivering higher average yields (6380 kg ha^{-1}) compared to the world's average yield (5930 kg ha^{-1}) [1].

Although China is one the largest maize producer worldwide, maize crops are distributed in a variety of climatic and ecological conditions with direct impacts over maize yields [2]. Since water deficit is one of the most important factors limiting crop yield stability [3] and most maize crops in China are rainfed [4], monitoring crop water status is crucial for decision making regarding agricultural management practices, especially in critical periods [3,5], in order to guarantee the larger stability and sustainability of agricultural systems.

Low levels of water availability affect a crop's physiological, biochemical and morphological traits, such as stomatal conductance, photosynthesis, intracellular CO_2 , chlorophyll, carotenoids, energy balance, aboveground biomass and yield [6–9]. The traditional methods for soil moisture monitoring (e.g., in loco collection of physical samples for soil gravimetric humidity determination) are laborious and time-consuming. Thus, vegetation water content has been used as a key indicator of the water relations in the soil–plant–atmosphere system, providing a faster and less expensive assessment of crop water status compared to traditional soil sampling methods [10].

However, soil moisture, and consequently vegetation water content, presents large spatiotemporal variability, and its sampling methods are point-based, which imposes limitations to near-real-time crop water status assessment in large areas [11,12]. In this context, remote sensing technology has been successfully used to monitor the water relations in the soil–plant–atmosphere system through canopy and leaf reflectance, contributing to the better management of water under precision agriculture practices [3] and the quantification of dynamic traits, such as growth conditions and leaf water content, based on time-series of non-laborious and non-destructive measurements in large areas [13,14].

Based on remote sensing approaches, vegetation water properties can be expressed in multiple definitions, and the majority of them consider different combinations of the turgid, fresh and dry weight of leaves, as well as leaf area, for its calculation. Thus, vegetation water content is often expressed as fuel moisture content (FMC), relative water content (RWC), equivalent water thickness (EWT), leaf/canopy water content (LWC/CWC) and gravimetric water content (GWC) for several crop types, including maize [8,14–16], soybean [9,17,18], wheat [3,19–22], and cotton [23,24].

From remote sensing perspectives, vegetation water status can be assessed via spectral information acquired from different platforms using ground-based sensors [9,14,21], multi and hyperspectral cameras attached to unoccupied aerial vehicles (UAVs) or airplanes [11,12,25], and satellites [26,27]. Currently, most retrieving methods using spectral data are based on the correlation between crop water properties and the reflectance from individual spectral bands (either narrowband or broadband reflectance), vegetation indices (either narrowband or broadband vegetation indices) computed from reflectance, and the use of the full reflectance spectra (either multispectral or hyperspectral) under multivariate or machine learning algorithms [7,18,22,24,28]. However, according to Ma et al. [29], the interaction of the visible, near-infrared, and shortwave infrared spectra (Vis–NIR–SWIR) with leaves and canopy might be different due to the influence from canopy structure, leaf area, angle, orientation, shadow, and background, which must be considered in the adoption of specific and effective spectral methods for vegetation water management. In this context, there is always a trade-off between spatial and spectral resolutions. Though ground-based sensors (e.g., spectroradiometer) have a higher spectral resolution, their use is a point-based method. On the other hand, while UAV-based sensors have the advantage of the rapid monitoring of large areas, they usually present a lower spectral resolution than spectroradiometers. Thus, simultaneously operating both ground- and UAV-based sensors might contribute to extract the best efficiency of each. Hence, considering the efficiency of both ground-based and UAV-based sensors for monitoring large agricultural

areas, the assessment of the spectral response at both levels is crucial for sustainable management practices.

Although both types of sensors are largely used for crop monitoring, the comparison of their efficiency in estimating leaf water content in similar spectral intervals (Vis–NIR) and the contribution of the SWIR spectral interval is not often reported. Hence, the present research was aimed to evaluate the performance of hyperspectral data collected at ground-based and UAV-based levels for maize leaf water content monitoring based on: (I) single wavelengths, (II) broadband reflectance and vegetation indices, (III) optimum hyperspectral vegetation indices, and (IV) the full maize spectrum using Partial Least Squares Regression.

2. Materials and Methods

2.1. Experimental Site

The experiment was conducted in the Shunyi Agro-Environmental Comprehensive Experimental Base, Institute of Environment and Sustainable Development in Agriculture from the Chinese Academy of Agricultural Sciences, Beijing, China (40°05'32" N, 116°55'07" E), in the 2020 cropping season. The collected data were analyzed following a split plot model in a randomized complete block design with three blocks. The following water condition treatments were distributed in the field plots: irrigation after sowing, irrigation after sowing and at the jointing stage, and irrigation after sowing at the jointing stage and at the tasseling stage. Maize varieties Jingke 968, Zhengdan 958 and Xianyu 335 were distributed in the subplots. The 27 experimental plots (50 m² each) were sown on 22 June 2020 and harvested from 16 October 2020.

2.2. Spectral Data Acquisition and Processing

Ground-based and UAV-based hyperspectral data were simultaneously collected at noon under cloud-free conditions at 64, 86 and 112 days after sowing (DAS). Although maize phenology might present differences among production areas, the assessed dates were established seeking to characterize maize crop close to the transition from the vegetative to reproductive phases, at the middle of reproductive stages, and close to maturation, following the work of Song et al. [30].

Leaf hyperspectral reflectance was collected from the central area of the adaxial face of upper third leaves using a FieldSpec 4 spectroradiometer (Analytical Spectral Devices, Boulder, CO, USA). To minimize possible within-field variability in the assessed plots, five plants were measured (one reflectance spectrum per plant) and reflectance values were averaged within each plot and each assessment date, resulting in the dataset used for LWC monitoring. After the spectral assessment, the evaluated leaves were immediately collected to determine the LWC, as described in Section 2.3.

The FieldSpec 4 spectroradiometer, with its plant probe accessory, has a spectral resolution of 3 nm between 350 and 1400 nm and 30 nm between 1400 and 2500 nm, and the output data are given in 2151 contiguous spectral bands of 1 nm width. The plant probe accessory has an internal 99% reflectance board (Spectralon[®], Labsphere, North Sutton, NH, USA), used as reflectance standard, and a 1% reflectance opaque and black board, which contributes to the collection of pure leaf reflectance spectra. Additionally, the plant probe accessory standardizes the illumination conditions and prevents external interferences and noises from adjacent targets, atmosphere scattering, and atmosphere attenuation without the need for spectral filters for noise removal and data smoothing [31].

Hyperspectral images were collected with a Pika-L hyperspectral push broom scanner (Resonon, Bozeman, MT, USA), with a spectral resolution of 2.1 nm between 400 nm and 1000 nm, mounted on an unoccupied aerial vehicle model DJI Matrice 600 Pro[®] Hexacopter (Shenzhen Dajiang Innovation Technology Co., Ltd., Shenzhen, China) with a GPS/IMU system for acquiring georeferenced images and further orthorectification procedures. Images were collected at 30 m of flight altitude and 80% and 70% of forward and lateral overlapping, respectively, delivering a spatial resolution of approximately 0.05 m. A camera stabilization system was used to avoid vibrations during the flight.

The collected hyperspectral images were processed through Spectron Pro Software (Resonon, Bozeman, MT, USA) and converted into reflectance through the use of ground-based hyperspectral reflectance from a calibration panel collected by an ASD spectroradiometer. A Savitzky–Golay smoothing filter was used for noise reduction (window size = 5 and polynomial order = 2), as suggested by Ge et al. [5], and bands under 424 nm and above 880 nm were excluded due to the presence of spectral noise and distortions [32], resulting in 120 spectral bands for LWC monitoring. Canopy vegetation pixels were masked and image backgrounds were excluded using an empirical threshold of >0.45 reflectance factor in the spectral band centered at 800 nm, as suggested by Feng et al. [32]. Within each plot, reflectance values from all canopy vegetation masked pixels (excluding pixels from the plot's edge) were extracted and averaged, resulting in the dataset used for LWC monitoring.

Figure 1 presents a representation of the spectral data acquisition using the ground-based (a) and UAV-based (b) sensors.



Figure 1. Spectral data acquisition using the ground-based (a) and UAV-based (b) sensors.

2.3. Leaf Water Content

Leaf water content was calculated, within each plot, from the average fresh mass and average dry mass of the five leaves used for hyperspectral assessment (Section 2.2), as per Equation (1):

$$\text{LWC (\%)} = \frac{W_{\text{fresh}} - W_{\text{dry}}}{W_{\text{dry}}} \times 100 \quad (1)$$

where W_{fresh} represents the fresh weight and W_{dry} represents the dry weight of a vegetation sample. The effectiveness of using fresh and dry weight for maize leaf water content under remote sensing perspectives was reported by Ge et al. [14] and Ge et al. [16]. The fresh weight was determined immediately after spectral assessment and leaf collection. Leaves were then placed in paper bags, taken to the laboratory, and dried at 70 °C for 24 h until dry weight was obtained [7].

2.4. Spectral Data Analysis

Four approaches were used to analyze the correlation between maize spectral response and leaf water content (LWC). To assess whether ground-based and UAV-based sensors presented consistent spectral responses for maize spectral characterization, the spectral curves from both sensors, on each assessment day, were plotted against each other, correlated, and evaluated via the Pearson coefficient of correlation (r).

2.4.1. Single Wavelengths for LWC Monitoring

To assess the potential of a single spectral band for LWC monitoring, spectral bands from the ground-based and UAV-based sensors were individually correlated to the corresponding LWC and evaluated with the Pearson coefficient of correlation (r). Additionally,

the coefficient of variation (CV) was calculated for each wavelength to assess the reflectance variability across the spectrum.

2.4.2. Broadband Reflectance and Vegetation Indices for LWC Monitoring

To evaluate the contribution of the broadbands and vegetation indices in providing competitive results for LWC monitoring, spectral data from both sensors were resampled to visible, near-infrared, and shortwave-infrared (Vis–NIR–SWIR) multispectral broadband resolutions [33] (Table 1), and broadband vegetation indices (VI) were calculated as per Table 2. Each resampled spectral band and calculated VI were individually correlated to LWC and evaluated with the Pearson coefficient of correlation (r).

Table 1. Characteristics of the broadband reflectance.

Spectral Band	Central Wavelength (nm)	Bandwidth (nm)
BLUE	492.4	66
GREEN	559.8	36
RED	664.6	31
RE ₁	704.1	15
RE ₂	740.5	15
RE ₃	782.8	20
NIR	832.8	106
SWIR ₁	1373.5	31
SWIR ₂	1613.7	91
SWIR ₃	2202.4	175

Table 2. Vegetation indices calculated from broadband reflectance.

Index	Formula	Reference
BNDVI	$BNDVI = \frac{(\rho^{NIR} - \rho^{Blue})}{(\rho^{NIR} + \rho^{Blue})}$	Wang et al. [34]
GNDVI	$GNDVI = \frac{(\rho^{NIR} - \rho^{Green})}{(\rho^{NIR} + \rho^{Green})}$	Gitelson et al. [35]
NDVI	$NDVI = \frac{(\rho^{NIR} - \rho^{Red})}{(\rho^{NIR} + \rho^{Red})}$	Rouse et al. [36]
NDRE ₁	$NDRE_1 = \frac{(\rho^{NIR} - \rho^{RE_1})}{(\rho^{NIR} + \rho^{RE_1})}$	Gitelson and Merzlyak [37]
NDRE ₂	$NDRE_2 = \frac{(\rho^{NIR} - \rho^{RE_2})}{(\rho^{NIR} + \rho^{RE_2})}$	Mehdaoui and Anane [38]
NDRE ₃	$NDRE_3 = \frac{(\rho^{NIR} - \rho^{RE_3})}{(\rho^{NIR} + \rho^{RE_3})}$	Mehdaoui and Anane [38]
NDWI	$NDWI = \frac{(\rho^{NIR} - \rho^{SWIR_1})}{(\rho^{NIR} + \rho^{SWIR_1})}$	Gao [39]
NDII	$NDII = \frac{(\rho^{NIR} - \rho^{SWIR_2})}{(\rho^{NIR} + \rho^{SWIR_2})}$	Hardisky et al. [40]
NDII 2	$NDII\ 2 = \frac{(\rho^{NIR} - \rho^{SWIR_3})}{(\rho^{NIR} + \rho^{SWIR_3})}$	Hardisky et al. [40]

2.4.3. Narrowband Vegetation Indices for LWC Monitoring

To investigate whether the selection of two optimum narrow hyperspectral bands could improve the accuracy of LWC monitoring, we calculated all possible combinations between two spectral bands under a normalized difference vegetation index formula (Equation (2)), as suggested by Ge et al. [14]. Each band combination (between two spectral bands under a normalized difference vegetation index formula) represents one hyperspectral vegetation index (HVI), and each HVI was then correlated to LWC and evaluated with the Pearson coefficient of correlation (r) and coefficient of determination (R^2) using a self-developed code in the IDL language. To enable intercomparison between both sensors at similar spectral intervals, the ground-based sensor was analyzed using the full spectra (from 400 nm to 2500 nm) and using Vis–NIR wavelengths (from 424 nm to 880 nm).

$$HVI = \frac{\text{Wavelength}_1 - \text{Wavelength}_2}{\text{Wavelength}_1 + \text{Wavelength}_2} \quad (2)$$

2.4.4. Partial Least Squares Regression (PLSR) for LWC Monitoring

To develop a hyperspectral prediction model comprising the full spectra, all bands from ground-based and UAV-based sensors were correlated to LWC using Partial Least Squares Regression (PLSR). Following the procedure adopted during the hyperspectral vegetation index analysis, the ground-based sensor was analyzed based on its full spectra (400 nm to 2500 nm) and Vis–NIR wavelengths (from 424 nm to 880 nm).

The PLSR is a multivariate regression method used to perform the linear correlation between spectral data (predictor variables) and leaf water content (response variables) through the selection of latent variables, and it has the advantage of dealing with the multi-collinearity usually found in hyperspectral data, which helps diminish model overfitting [13]. As a result, the spectral data were transformed into a linear model composed of waveband scaling coefficients [41]. PLSR ($p \leq 0.05$) was performed by the Unscrambler® (CAMO Software, Oslo, Norway) based on the optimal number of latent variable, as indicated by the lowest value of root mean square error (RMSE) through the leave-one-out cross-validation method, the highest coefficient of determination (R^2) of multivariate regression, and the value of systematic error (BIAS) close to zero [42]. The accuracy of the PLSR models was assessed with the Pearson coefficient (r) and the coefficient of determination (R^2) from the linear regression between observed and predicted LWC during the leave-one-out cross-validation procedure.

3. Results and Discussion

3.1. Maize Leaf Water Content

Figure 2 presents the measured maize leaf water content on the three assessment days. The highest values of LWC were observed at 64 DAS, ranging from 74% to 79%. Lower values were observed at 86 and 112 DAS, ranging from 70% to 75% and from 71% to 76%, respectively.

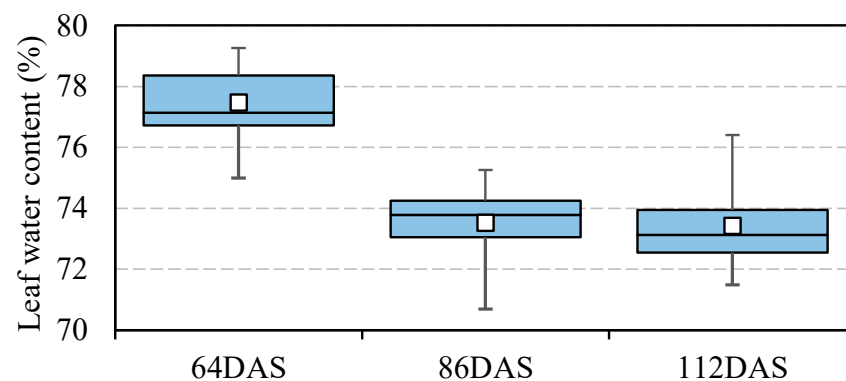


Figure 2. Boxplot of maize leaf water content.

3.2. Maize Leaf and Canopy Reflectance

The average maize reflectance collected on the three field assessments using the ground-based (leaf reflectance) and UAV-based (canopy reflectance) sensors is presented in Figure 3. Both canopy and leaf-based sensors presented similar shapes of maize spectral behavior, with differences in the reflectance intensity among the assesses dates.

At the first assessment day (64 DAS), the UAV-based sensor demonstrated lower reflectance across visible wavelengths, and the reflectance in the near-infrared spectrum was higher than that of the ground-based sensor. At 86 DAS (second assessment day), a larger similarity between both sensors was observed across the visible spectrum, mainly between 500 and 680 nm. However, as in the previous assessment day, a higher reflectance in the near-infrared was observed at the canopy level (UAV-based) compared to the leaf level (ground-based sensor). At the last assessment day (112 DAS), the reflectance acquired at the canopy level (UAV-based sensor) presented higher values compared to the leaf level

between 560 and 680 nm and the spectral behavior at the near-infrared was kept, with a higher reflectance at the canopy level.

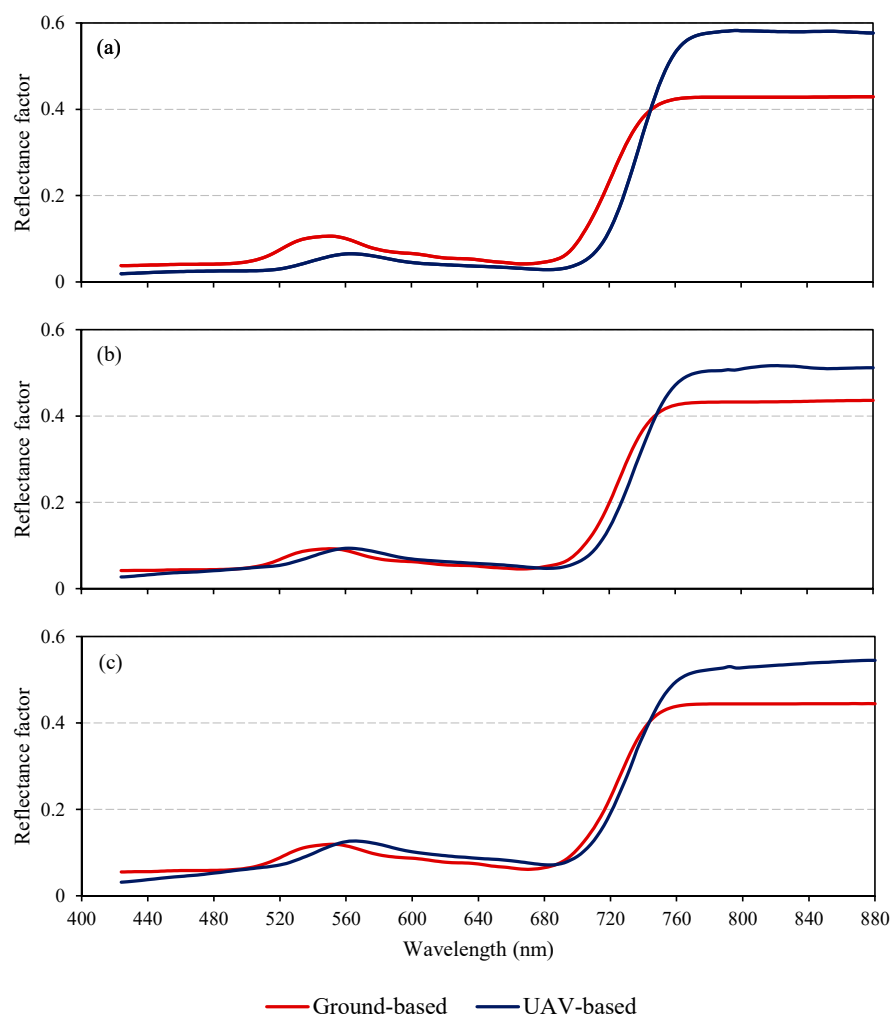


Figure 3. Average maize reflectance measured from the ground-based and UAV-based sensors at 64 DAS (a), 86 DAS (b) and 112 DAS (c).

Canopy background and shadows might decrease the reflectance across a spectrum, resulting in about only 40–70% reflectance compared to that at the leaf level [27,29]. However, the masking of vegetation pixels performed in the hyperspectral images enabled the acquisition of just the vegetation spectra, thus providing similar shapes in the spectral response at both levels of spectral data acquisition.

According to Ma et al. [29], effects derived from leaf orientation, leaf area and canopy architecture make the analysis of canopy reflectance more complex compared to that of leaf reflectance. Additionally, leaves at different ages might present different spectral responses, mainly influenced by the absorption of photosynthetic active radiation [43]. Addressing the monitoring of water-related properties using remote sensing data, Liu et al. [19] described the light attenuation by scattering and absorption per unit distance through the canopy due to leaf angle and canopy depth, and they highlighted that this attenuation was not constant along the canopy and wavelengths and, in maize crop, might also have been affected by the bell-shaped vertical distribution of biophysical properties.

Although differences in reflectance intensity were observed across the Vis–NIR spectrum, with small differences across the visible spectrum and larger differences in the near-infrared wavelengths, the shape of the spectral curve acquired at both levels was demonstrated to be similar, with a coefficient of correlation of over 0.97 between ground-

based and UAV-based sensors on the three assessment days, indicating the potential of comparing their performance for maize leaf water content monitoring.

Considering the similar response from both sensors regarding maize spectral behavior, it was possible to further analyze the relation between spectral data and LWC. Although differences in reflectance were observed, the consistency in the obtained spectral data contributed to the demonstration of how both sensors could be complementarily used and allowed us to compare their performance for leaf water content monitoring under the four approaches used.

Hence, the importance of comparing the performance of ground-based and UAV-based sensors for maize LWC monitoring relies on the need for the adoption of specific methods for each sensor and monitored area [29], as well as the possibility of integrating both sensors, considering the potential contained in their spectral response [44]. Thus, the development of methods and parameters for the accurate spatial and temporal monitoring of crop LWC will optimize extrapolation to large-scale target areas.

The advantage of using ground-based sensors is their potential for the detailed analyses of specific leaves, with a higher spectral resolution, which might contribute to the acquisition of more robust spectral models. However, this is a point-based method, which might impose limitations to the monitoring of large crop areas and the extrapolation of the developed spectral models. On the other hand, UAV-based sensors, despite their lower spectral resolution, has the advantage of time efficiency when capturing images of large crop areas, contributing to the extrapolation of the developed spectral models for LWC monitoring.

3.3. Single Wavelengths for LWC Monitoring

Figure 4 presents the correlation between maize leaf water content and canopy reflectance measured by the UAV-based hyperspectral sensor and the coefficient of variation (CV) of the reflectance across the spectrum. Different shapes of correlation between LWC and reflectance across the visible spectrum were observed on the three assessment days, and the maximum negative correlation was observed in the near-infrared spectrum.

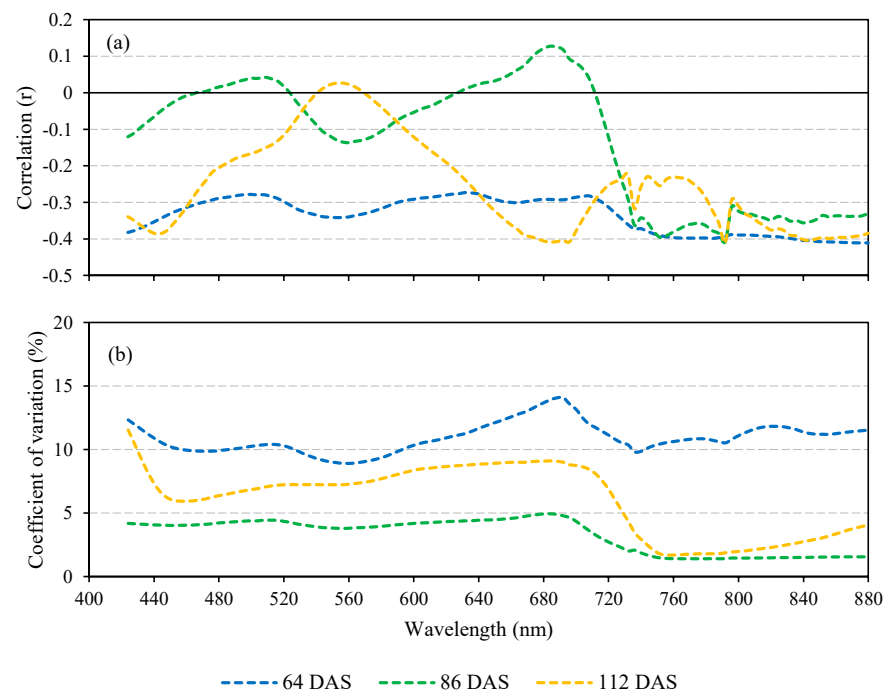


Figure 4. Correlation between maize leaf water content and canopy reflectance (a) and the coefficient of variation across the spectrum (b).

At 64 DAS, negative correlations were observed between LWC and canopy reflectance across the Vis–NIR spectrum, reaching maximum values ($r > -0.39$) across near-infrared wavelengths from 752 to 880 nm. However, at 86 DAS, the correlation curve demonstrated a different pattern, with positive correlations observed from 468 to 520 nm and from 628 to 708 nm. Following the results observed at 64 DAS, negative correlations reached their maximum values ($r > -0.38$) from 748 to 880 nm. At the third assessment day, 112 DAS, positive correlations were also observed across the visible spectrum between 544 and 568 nm, while the negative correlations reached their maximum values ($r > -0.32$) from 732 to 880 nm.

Although positive correlations were not expected to be observed between leaf water content and reflectance, many authors have reported this behavior when analyzing canopy reflectance data. Using canopy reflectance derived from airborne hyperspectral images over a heterogeneous vegetation area, Al-Moustafa et al. [12] reported positive correlations between LWC and wavelengths of between 700 nm and 1100 nm. Similarly, El-Hendawy et al. [3], Liu et al. [19] and Zhang et al. [22] observed positive correlations between wheat LWC and reflectance between 700 nm and 1300 nm using a canopy-based hyperspectral sensor. Yi et al. [24], addressing the monitoring of LWC in cotton with a leaf-based hyperspectral sensor, reported positive correlations around 450 nm and 550 nm, as well as between 675 nm and 1400 nm.

Unlike the correlation curve, the coefficient of variation presented similar trends on the three assessment days, with differences in their magnitudes. In general, higher CV values were observed at 64 DAS, followed by 112 DAS and 86 DAS. For all assessment days, the highest values of CV were observed from 684 to 692 nm and the lowest CV values were observed across the near-infrared spectrum from approximately 740 nm.

Figure 5 presents the correlation between maize leaf water content and leaf reflectance measured by the ground-based hyperspectral sensor and the coefficient of variation (CV) of reflectance across the spectrum. Differently from the UAV-based sensor, a trend in the correlation between LWC, leaf-based reflectance, and the CV curve was observed. As expected, differently from the UAV-based sensor, negative correlations between LWC and reflectance were observed across the spectrum in the three assessment dates.

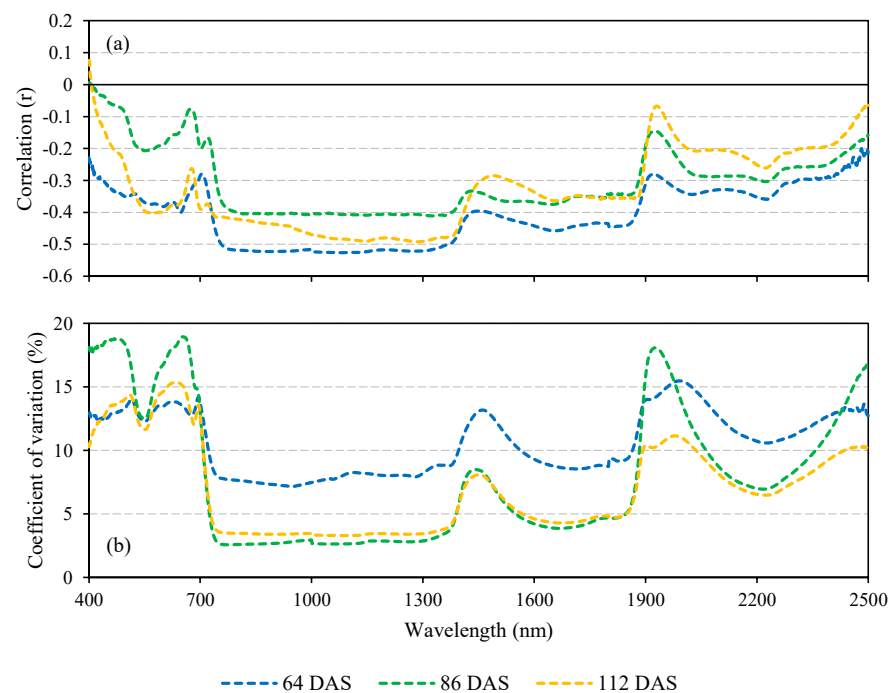


Figure 5. Correlation between maize leaf water content and leaf reflectance (a) and the coefficient of variation across the spectrum (b).

In all assessment days, negative correlations between leaf reflectance and leaf water content were observed across the spectrum, with the highest correlations observed across NIR. Although the correlation between leaf reflectance and maize leaf water content was demonstrated to be constant in NIR, the highest correlations were observed at the transition between the NIR and SWIR wavelengths: 1069 nm ($r = -0.53$), 1327 nm ($r = -0.41$) and 1283 nm ($r = -0.49$) at 64, 86 and 112 DAS, respectively.

Across the visible wavelengths, the highest correlations were observed at 647 nm ($r = -0.40$), 551 nm ($r = -0.21$) and 571 nm ($r = -0.40$) at 64, 86 and 112 DAS, respectively, with inflexions across the blue and red wavelengths. Across the SWIR wavelengths, the highest correlations were observed between 1300 nm and 1850 nm, decreasing towards 2500 nm and with inflexions in the correlation curve around 1400 nm and 1900 nm.

The CV curves across the spectrum demonstrated similar shapes to the correlation curves. Although the NIR wavelengths demonstrated the highest correlation to LWC, this spectral interval presented the lowest CV across the spectrum. The SWIR wavelengths showed intermediate CV values, with highest values at 1990 nm, 1924 nm and 1981 nm at 64, 86 and 112 DAS, respectively. In general, similar CV values were observed across the visible wavelengths, with higher values across blue and red spectral intervals compared to the green intervals.

The lack of pattern in the correlation between the single band from the UAV-based sensor and maize leaf water content across cropping season might have been related to the large spatial and temporal variability of vegetation water content, largely influenced by crop physiology, soil properties and atmosphere conditions [12]. In the same context, vegetation water content might also present vertical variability among leaves. Accordingly, the estimation of vegetation properties by the UAV-based sensor may be affected by the differential distribution of light through a canopy due to leaf angle and the amount of reflected light [19]. Additionally, the overall condition of leaf water content within the experimental plots might not be fully represented by the leaves used for LWC determination, leading to mismatch with the canopy reflectance.

Different from the UAV-based sensors, subjected to the influence of atmospheric and illumination conditions [45], the ground-based hyperspectral sensor demonstrated a consistent trend in the three days of spectral assessments in the correlation between reflectance and LWC. Leaf-based sensors have the advantage of preventing illumination interferences from adjacent targets, atmospheric scattering, and atmospheric attenuation. Thus, considering that leaf-based spectral measurements were performed in the same leaves used for LWC, a better fit between spectral response and LWC could be achieved compared to canopy reflectance.

As a result of lower levels of water availability, and consequently lower leaf water contents, an increase in reflectance was observed across the Vis–NIR–SWIR spectrum, with differences across wavelengths due leaf biochemical properties and structure [46]. Variations in leaf water content result in primary and secondary effects on leaf reflectance. The primary effects are related to the absorption of radiation by water, affecting the reflectance across the SWIR spectrum [20,43,47].

The secondary effects cannot be solely explained by the absorption of radiation by water [20] and are indirectly associated with the leaf water content. The secondary effects are largely expressed across visible wavelengths, associated with leaf pigments and the absorption of photosynthetic active radiation [3,47], and across near-infrared wavelengths, associated with the light scattering along the mesophyll and influenced by internal leaf structures such as cell wall widths, intercellular air spaces, and the amount of mesophyll per unit of leaf area [20,47].

Although the highest correlations between leaf reflectance and LWC were observed across the NIR wavelengths (Figures 4a and 5a), the coefficient of variation of this spectral interval was demonstrated to be lower compared than those of the Vis and SWIR wavelengths (Figures 4b and 5b). Accordingly, Ronay et al. [8] stated that the Vis and SWIR wavelengths have larger sensibilities to leaf water content compared to NIR. In the

same context, Ullah et al. [13] emphasized that the absorption of incident radiation by water molecules in leaves is weak in NIR and strong in SWIR. Using leaf-based reflectance from a hyperspectral sensor to monitor LWC in maize plants, Zygielbaum et al. [15] reported a larger sensibility across visible and shortwave infrared wavelengths. Carter [47] demonstrated that a lower sensitivity to LWC was found across NIR (between 700 nm and 1300 nm) due to the low absorbance of radiation by water and that a larger sensibility could be found across Vis (around 480 nm and 680 nm) and SWIR (mainly around 1450 nm, 1920 nm and 2500 nm). Complementarily, the authors of this study demonstrated that the secondary effects of LWC across visible spectrum could present similar or even larger magnitudes to the primary effects of LWC across SWIR, corroborating the results shown in Figures 4b and 5b.

3.4. Broadband Reflectance and Vegetation Indices for LWC Monitoring

Figure 6 presents the correlation between maize leaf water content, spectral bands, and the derived vegetation indices (Table 2) using the ground-based (a) and UAV-based (b) sensors.

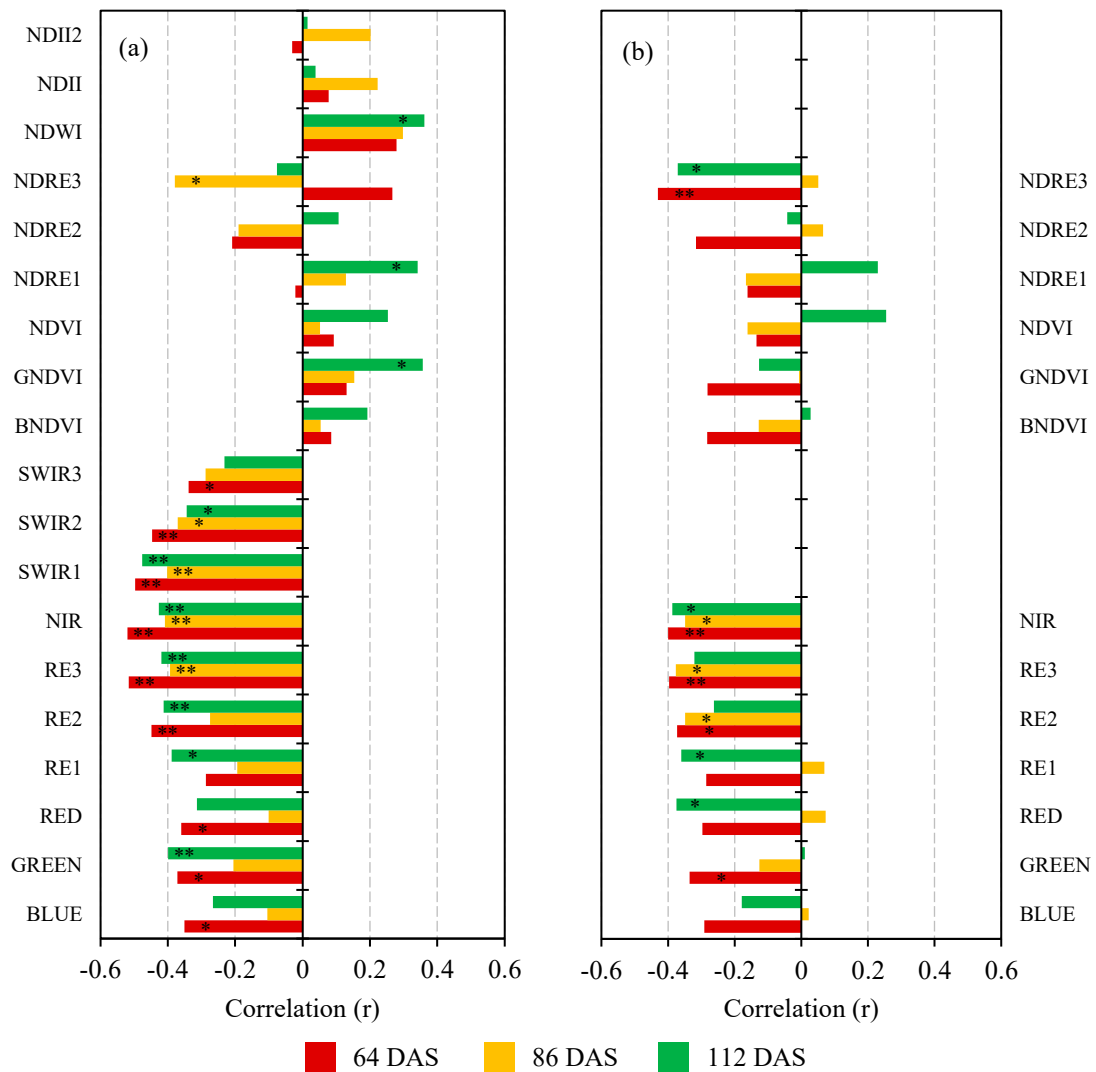


Figure 6. Correlation between maize leaf water content and spectral bands and derived vegetation indices using the ground-based (a) and UAV-based (b) sensors. * Significant at 0.10 α , ** Significant at 0.05 α .

Similar patterns were observed for both sensors regarding the use of spectral bands, with negative correlations between maize LWC and spectral bands except for the blue, red and red-edge1 bands at 86 DAS from the canopy reflectance. Using spectral data from the ground-based sensor, the highest correlations were found for the NIR band at 64 DAS ($r = -0.52$) and 86 DAS ($r = -0.41$), as well as for SWIR1 band ($r = -0.48$) at 112 DAS. Using spectral data from the UAV-based sensor, the highest correlations were observed for the NIR band at 64 DAS ($r = -0.40$) and 112 DAS ($r = -0.39$), as well as for the red-edge3 band at 86 DAS ($r = -0.39$).

Broadbands derived from ground-based and UAV-based sensors were demonstrated to be negatively correlated to leaf water content, with higher correlations for the leaf-based sensor. The negative trend between broadband reflectance and LWC is corroborated by the vegetation spectral behavior under variations of LWC, with increasing reflectance across the Vis–NIR–SWIR spectrum in leaves with lower water status [46], as discussed in Section 3.3.

Addressing the correlation between LWC and vegetation indices, a different trend was observed between the ground-based and UAV-based sensors: though positive correlations with LWC were generally observed when using leaf reflectance, most of the vegetation indices were demonstrated to be negatively correlated to LWC when using canopy reflectance. For the ground-based sensor, the outstanding VIs were NDWI at 64 DAS ($r = 0.28$) and 112 DAS ($r = 0.36$), as well as NDRE3 ($r = -0.38$) and NDWI ($r = 0.30$) at 86 DAS. For the UAV-based sensor, the outstanding VIs were NDRE3 at 64 DAS ($r = -0.43$) and 112 DAS ($r = -0.37$), as well as NDRE1 ($r = -0.17$) at 86 DAS.

According to Sakamoto [48], vegetation indices derived from images are usually used based on their direct relationship with biomass and indirect relationship between biomass and crop agronomic parameters. Considering that the background (soil and shadows) was removed from the hyperspectral images, a low correlation could be observed between UAV-based VIs and LWC. Ge et al. [14], considering maize LWC monitoring using canopy-based hyperspectral sensor, also obtained low correlations with broadband vegetation indices. Additionally, the positive correlation observed in this study between UAV-based data and LWC might have been affected by the variation in light distribution through the canopy, complex reflectance from different leaves, and a mismatch between the overall LWC condition and the collected leaves for LWC determination within each field, as suggested in Section 3.3.

3.5. Narrowband Vegetation Indices for LWC Monitoring

Figure 7 presents the map of coefficient of correlation (R^2) from the linear regression between LWC and all possible combinations between two narrow hyperspectral bands to calculate the hyperspectral vegetation indices (Equation (2)) using the UAV-based and ground-based sensors. At this stage, spectral data from the ground-based sensor were analyzed using the full spectra (400–2500 nm) and the similar spectral interval from the UAV-based sensor (424–880 nm).

When using the UAV-based sensor, the best spectral intervals for band combination were NIR/NIR (64 DAS), red-edge/red-edge (86 DAS) and Vis/Vis (112 DAS). When using the ground-based sensor within the same spectral interval, Vis/Vis band combinations showed the highest values of R^2 . When investigating the band combination within the Vis/NIR/SWIR spectrum, SWIR/SWIR combinations demonstrated the highest R^2 on the three assessment days, with intermediate results from NIR/NIR at 64 DAS and Vis/Vis and Vis/SWIR at 112 (DAS).

El-Hendawy et al. [3], addressing the correlation between wheat LWC and hyperspectral vegetation indices derived from a canopy-based sensor, stated that the success of hyperspectral vegetation index development is dependent on the use of bands with different sensitivities to the key parameter to be monitored. According to the authors, band combinations between Vis/NIR, NIR/NIR and NIR/SWIR outperform Vis/Vis and Vis/SWIR. Complementarily, Mirzaie et al. [7], performing LWC estimation on multiple

plant species with hyperspectral vegetation indices, suggested that the shortwave infrared spectrum has many band combinations with high correlations.

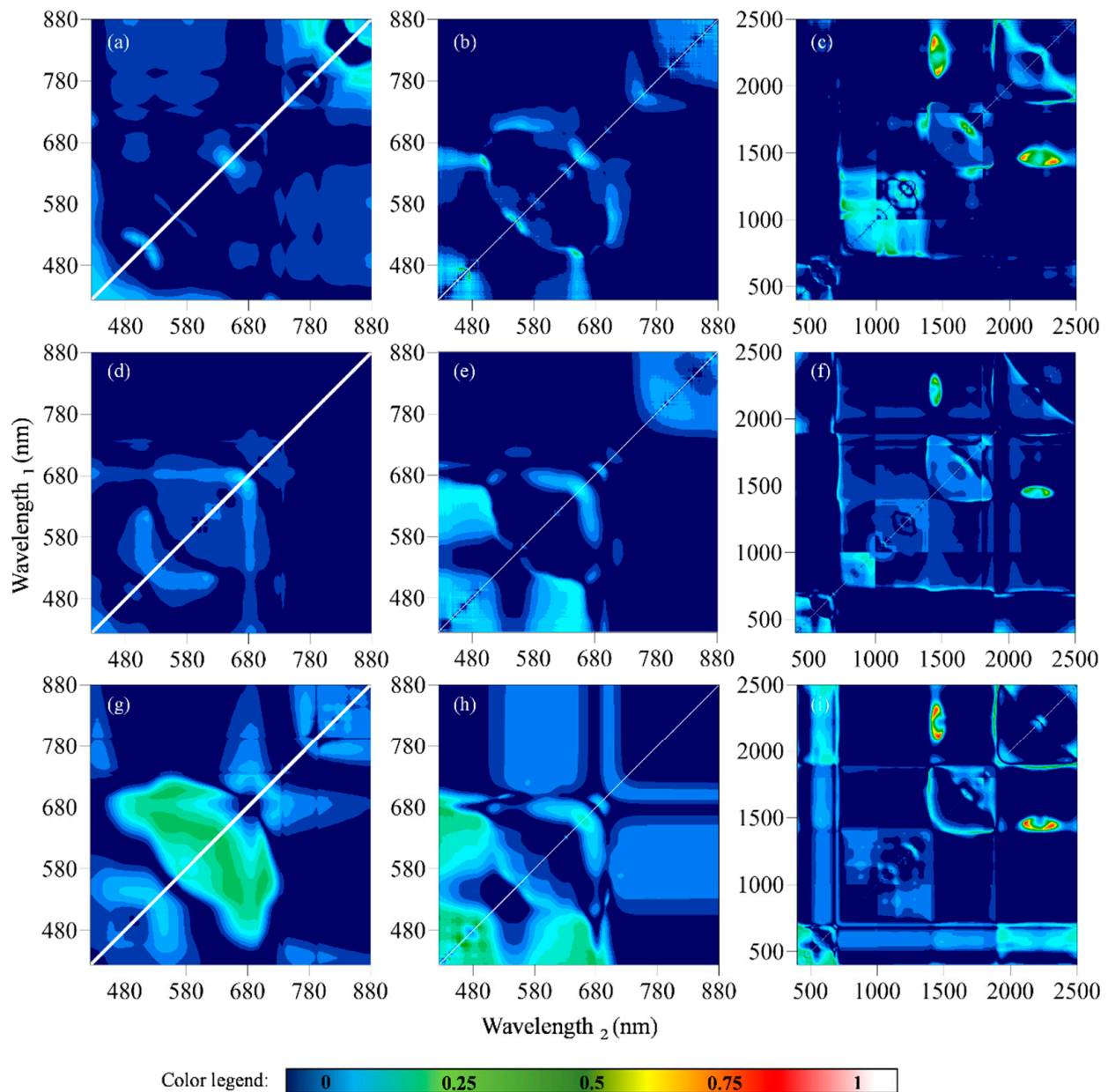
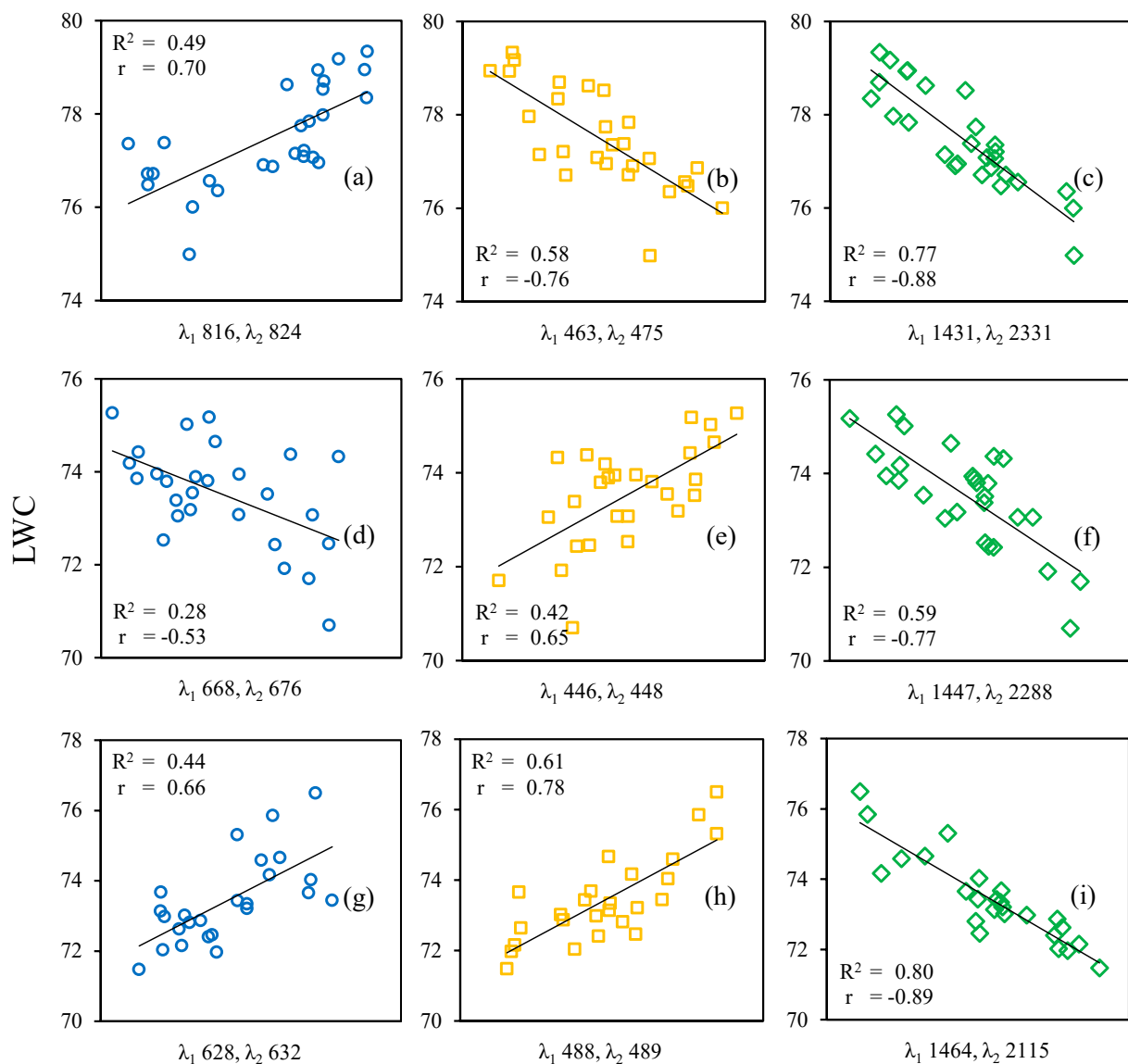


Figure 7. Map of coefficient of correlation (R^2) from the linear regression between LWC and all possible band-to-band combinations to calculate the hyperspectral vegetation indices (Equation (2)) using: the UAV-based sensor at 64 (a), 86 (d) and 112 DAS (g); the ground-based sensor from 424 to 880 nm at 64 (b), 86 (e) and 112 DAS (h); and the ground-based sensor from 400 to 2500 nm at 64 (c), 86 (f) and 112 DAS (i).

Figure 8 presents the correlation between maize leaf water content and the optimum band combination for the hyperspectral vegetation index (Equation (2)) derived from Figure 7.

A consistent pattern was observed when analyzing the spectral data within the Vis-NIR spectral interval (UAV-based and ground-based—424–880 nm—sensors): in all days, the selected bands for each sensor were demonstrated to be closely related to each other or even contiguous. For the UAV-based sensor, the optimum band combinations were 816 nm and 824 nm (64 DAS—Figure 8a), 668 nm and 676 nm (86 DAS—Figure 8d), and

628 nm and 632 nm (112 DAS—Figure 8g), and the optimum band combinations using leaf reflectance (from 424 nm to 880 nm) were 463 nm and 475 nm (64 DAS—Figure 8b), 446 nm and 448 nm (86 DAS—Figure 8e), and 488 nm and 489 nm (112 DAS—Figure 8h). Meanwhile, the optimum band combination for the ground-based sensor (424–880 nm) was demonstrated to be located around blue wavelengths, within 44 nm (from 446 nm to 489 nm), and the optimum band combination for the UAV-based sensor was demonstrated to be located around either the red and near-infrared wavelengths.



Optimum band combination

Figure 8. Correlation between maize leaf water content and the optimum band combination for the hyperspectral vegetation index calculation using: the UAV-based sensor at 64 (a), 86 (d) and 112 DAS (g); the ground-based sensor from 424 to 880 nm at 64 (b), 86 (e) and 112 DAS (h); and the ground-based sensor from 400 to 2500 nm at 64 (c), 86 (f) and 112 DAS (i).

When analyzing the spectral data within the Vis–NIR–SWIR spectral interval (ground-based sensor, full spectra 400–2500 nm), however, a consistent pattern was observed: band 1 (wavelength 1) was located within the 1431–1464 nm spectral interval and band 2 (wavelength 2) was located within the 2115–2331 nm in the three assessment days. The

optimum band combinations were 1431 nm and 2331 nm (64 DAS—Figure 8c), 1447 nm and 2288 nm (86 DAS—Figure 8f), and 1464 nm and 2115 nm (112 DAS—Figure 8i).

For the calculated HVI, the position of the two optimal spectral bands for LWC monitoring in Equation (2) determined the tendency (positive or negative) for the correlation between LWC and the HVI. If the position of the selected wavelengths was changed, the R^2 remained equal but a different tendency was observed. This can be demonstrated by the mirror formed by the 1:1 line in Figure 7. In the presented results, the position of the selected bands was standardized, designating the smaller wavelength as ‘Wavelength₁’ and the larger wavelength as ‘Wavelength₂’, as shown in Figure 8. In this context, optimum band combinations were found to be centered in the SWIR wavelengths for LWC monitoring in multiple plant species (1400 nm and 1600 nm—Ullah et al. [13]; 1410 nm and 1830 nm—Cao et al. [28]), including the cotton crop (1645 nm and 1693 nm—Yi et al. [24]). Performing a high-throughput analysis of leaf water content with Vis–NIR–SWIR spectroscopy within a maize diversity panel, Ge et al. [14] found the optimum hyperspectral vegetation index at bands 1465 nm and 2125 nm, centered in the same spectral interval as the optimum HVI obtained in this study at 64, 86 and 112 DAS (Figure 8c,f,i).

Using canopy reflectance (UAV-based sensor), the optimal band combination delivered R^2 from 0.28 to 0.49, with coefficients of correlation equal to 0.70 (64 DAS), -0.53 (86 DAS) and 0.66 (112 DAS). Using leaf reflectance within the same spectral interval, the optimal band combination delivered higher values of R^2 from 0.42 to 0.61, with coefficients of correlation equal to -0.76 (64 DAS), 0.65 (86 DAS) and 0.78 (112 DAS). The highest values of R^2 , ranging from 0.59 to 0.80, were obtained using the leaf-based reflectance within the Vis–NIR–SWIR spectrum, with coefficients of correlation equal to -0.88 (64 DAS), -0.77 (86 DAS) and -0.89 (112 DAS).

The accuracy of LWC monitoring using HVI was demonstrated to be higher than that of single band reflectance, broadband reflectance, and vegetation indices. The advantage of HVI over broadband VIs relies on the loss of important spectral information when the spectral intervals used to calculate the broadband vegetation indices are enlarged. Since hyperspectral vegetation indices use narrow spectral bands, it becomes possible to identify key spectral features that represent specific biophysical or biochemical parameters of vegetation (e.g., leaf water content). Compared to single spectral bands or broadband reflectance, HVI is more suitable for capturing differences with a higher sensitivity. Furthermore, HVI has the advantage of minimizing the spectral redundancy usually found in hyperspectral data and also promotes computational optimization [6,14,23]. In this context, Cao et al. [28] discussed the influence of band width on the estimation of vegetation water-related properties, emphasizing a decrease in accuracy when enlarging the band width. Yi et al. [24] reported a higher accuracy of HVI compared to broadband VI for the LWC monitoring of cotton plants.

3.6. Partial Least Squares Regression Models for LWC Monitoring

Figure 9 presents the PLSR results for maize LWC monitoring using the UAV-based and ground-based sensors. At this stage, the spectral data from the ground-based sensor were analyzed using the full spectra (400–2500 nm) and the similar spectral interval from the UAV-based sensor (424–880 nm).

Following the trend observed in Section 3.5, the use of leaf-based reflectance presented better results on the three assessment days compared to the use of canopy reflectance, and the analysis of the full Vis–NIR–SWIR spectra delivered the best results.

PLSR models using canopy reflectance (UAV-based sensor) for LWC monitoring delivered R^2 from 0.05 to 0.45, with coefficients of correlation equal to 0.67 (64 DAS), 0.21 (86 DAS) and 0.52 (112 DAS). Using leaf reflectance within the same spectral interval, PLSR models delivered higher values of R^2 from 0.13 to 0.63, with coefficients of correlation equal to 0.79 (64 DAS), 0.36 (86 DAS) and 0.55 (112 DAS). The full spectra of leaf reflectance (Vis–NIR–SWIR) delivered the highest values of R^2 ranging from 0.48 to 0.76, with coefficients of correlation equal to 0.87 (64 DAS), 0.69 (86 DAS) and 0.79 (112 DAS).

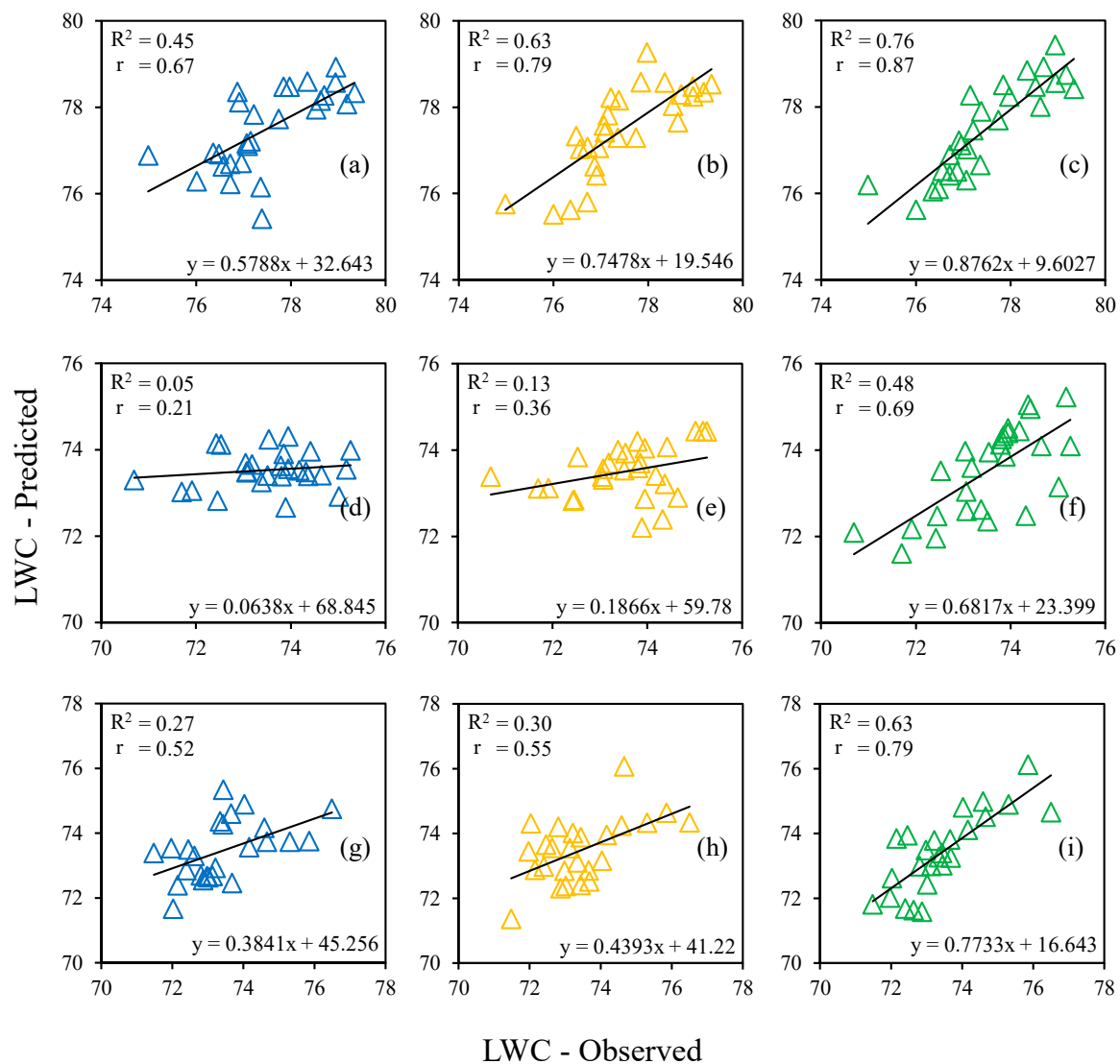


Figure 9. Results from PLSR for maize water content using: the UAV-based sensor at 64 (a), 86 (d) and 112 DAS (g); the ground-based sensor from 424–880 nm at 64 (b), 86 (e) and 112 DAS (h); and the ground-based sensor from 400–2500 nm at 64 (c), 86 (f) and 112 DAS (i).

PLSR demonstrated better performance in the monitoring of LWC compared to the single wavelength correlation or broadband spectral bands and vegetation indices. However, the results from the hyperspectral vegetation index demonstrated better performance than PLSR.

The potential of using PLSR for maize trait monitoring through UAV-based and ground-based spectral data was reported by Ge et al. [14], Shu et al. [6] and Yendrek et al. [41], and the outperformance of PLSR in relation to single wavelengths and broadband reflectance and vegetation indices for plant traits estimation has been largely demonstrated [3,7,13].

However, although PLSR has been suggested to outperform the use of hyperspectral vegetation indices [3,7,13,14], competitive results between both methods have also been reported [7,22]. Though PLSR has the advantage of dealing with multicollinearity, enabling the input of hundreds of spectral bands into the same model (weighting them according to their contribution as key spectral features for trait monitoring [13,41]), the simplicity of hyperspectral indices and computational advantages [7,14] demonstrate their potential for LWC monitoring. Hence, a specific HVI might be used as a benchmark in spectral analysis, guaranteeing a minimum loss of spectral information compared to full spectrum methods

and contributing to the development of new multispectral sensors and methods centered on key spectral features [44].

Based on the obtained results, the assessed spectral techniques demonstrate potential for maize leaf water content monitoring. We recommend further research of the variability among different locations and different years. The choice of the technique to be used will depend on the extension of the study area and the spatial variability to be characterized, the frequency of spectral information needed to be acquired across cropping seasons, and the availability of sensors (multispectral or hyperspectral) operated at the ground and aerial levels. Among the assessed spectral techniques, future investigations should focus on the use of hyperspectral vegetation indices and full spectrum models such as PLSR.

4. Conclusions

In this research, we evaluated the performance of hyperspectral data collected at the ground-based and UAV-based levels for maize leaf water content monitoring. Both sensors demonstrated similar shapes in the spectral responses from the leaves and canopy, though difference between them could be detected (mainly across the near-infrared spectrum). The correlation between spectral response and leaf water content was demonstrated to be higher using leaf-based reflectance than canopy-based reflectance. Specifically, the use of the full spectra (Vis–NIR–SWIR) was demonstrated to outperform the use of Vis–NIR spectra.

Among the four approaches for maize leaf water content monitoring, the best results were obtained using hyperspectral vegetation indices and Partial Least Squares Regression models. The developed hyperspectral vegetation indices proved to be suitable for LWC monitoring, delivering competitive or even better results compared to multivariate models using the full spectra (PLSR).

The optimal band combinations for hyperspectral vegetation indices using the UAV-based sensor were centered between 628 nm and 824 nm, with R^2 ranging from 0.28 to 0.49, while using the ground-based sensor the optimal band combinations for hyperspectral indices were consistently located around 1431–1464 nm (band 1) and 2115–2331 nm (band 2), with R^2 ranging from 0.59 to 0.80.

The obtained results indicate the potential of using ground-based and UAV-based hyperspectral data for maize LWC monitoring and indicate the possibility of the complementary use of both sensors, enabling the development of spectral models in loco using the ground-based sensor and extrapolating those models to larger crop areas using the UAV-based sensor for leaf water content mapping.

Although the efficiency of ground- and UAV-based sensors for LWC monitoring in maize crops has been demonstrated, especially using PLSR and HVI, the need for future research aiming performing a larger number of spectral assessments across cropping seasons, enhancing the understanding of reflectance–LWC dynamic across time, is highlighted. Additionally, it is important to enlarge the number of seasons to be monitored, providing performance assessment in years with different effects from the environment. To conclude, spectral assessment in different production areas, with different soil and climate properties, will contribute to strength the characterization of water-related properties in a larger gradient of growth environment.

Author Contributions: Conceptualization, L.G.T.C. and L.S.; methodology, L.G.T.C., L.S., Z.S. and R.C.; data acquisition, L.G.T.C., L.S., Z.S., R.C., Y.W., J.M. and C.S.; software, L.G.T.C. and Z.S.; formal analysis, L.G.T.C.; data curation, L.G.T.C. and L.S.; writing—original draft preparation, L.G.T.C. and L.S.; project administration, L.S.; funding acquisition, L.S. All authors have read and agreed to the published version of the manuscript.

Funding: This research was funded by the Science and technology innovation project of the Chinese Academy of Agricultural Sciences (Grant No. G202120-5); the Talented Young Scientist Program—China Science and Technology Exchange Center [Brazil-19-004]; and the Central Public-Interest Scientific Institution Basal Research Fund [Y2021GH18].

Institutional Review Board Statement: Not applicable.

Informed Consent Statement: Not applicable.

Data Availability Statement: The data that support the findings of this study are available from the author L.G.T.C.

Conflicts of Interest: The authors declare no conflict of interest.

References

1. United States Department of Agriculture (USDA). World Agricultural Production. Circular Series WAP 8–21 August 2021. 2021. Available online: <https://apps.fas.usda.gov/PSDOnline/Circulars/2021/08/production.pdf> (accessed on 20 September 2021).
2. He, H.; Hu, Q.; Li, R.; Pan, X.; Huang, B.; He, Q. Regional gap in maize production, climate and resource utilization in China. *Field Crops Res.* **2020**, *254*, 107830. [[CrossRef](#)]
3. El-Hendawy, S.E.; Al-Suhaibani, N.A.; Elsayed, S.; Hassan, W.M.; Dewir, Y.H.; Refay, Y.; Abdella, K.A. Potential of the existing and novel spectral reflectance indices for estimating the leaf water status and grain yield of spring wheat exposed to different irrigation rates. *Agric. Water Manag.* **2019**, *217*, 356–373. [[CrossRef](#)]
4. Meng, Q.; Hou, P.; Wu, L.; Chen, X.; Cui, Z.; Zhang, F. Understanding production potentials and yield gaps in intensive maize production in China. *Field Crops Res.* **2013**, *143*, 91–97. [[CrossRef](#)]
5. Ge, X.; Wang, J.; Ding, J.; Cao, X.; Zhang, Z.; Liu, J.; Li, X. Combining UAV-based hyperspectral imagery and machine learning algorithms for soil moisture content monitoring. *PeerJ* **2019**, *7*, e6926. [[CrossRef](#)] [[PubMed](#)]
6. Shu, M.; Shen, M.; Zuo, J.; Yin, P.; Wang, M.; Xie, Z.; Tang, J.; Wang, R.; Li, B.; Yang, X.; et al. The Application of UAV-Based Hyperspectral Imaging to Estimate Crop Traits in Maize Inbred Lines. *Plant Phenomics* **2021**, *2021*, 9890745. [[CrossRef](#)] [[PubMed](#)]
7. Mirzaie, M.; Darvishzadeh, R.; Shakiba, A.; Matkan, A.A.; Atzberger, C.; Skidmore, A. Comparative analysis of different uni- and multi-variate methods for estimation of vegetation water content using hyper-spectral measurements. *Int. J. Appl. Earth. Obs.* **2014**, *26*, 1–11. [[CrossRef](#)]
8. Ronay, I.; Ephrath, J.E.; Eizenberg, H.; Blumberg, D.G.; Maman, S. Hyperspectral Reflectance and Indices for Characterizing the Dynamics of Crop–Weed Competition for Water. *Remote Sens.* **2021**, *13*, 513. [[CrossRef](#)]
9. Kovar, M.; Brestic, M.; Sytar, O.; Barek, V.; Hauptvogel, P.; Zivcak, M. Evaluation of hyperspectral reflectance parameters to assess the leaf water content in soybean. *Water* **2019**, *11*, 443. [[CrossRef](#)]
10. Zhou, H.; Zhou, G.; He, Q.; Zhou, L.; Ji, Y.; Lv, X. Capability of leaf water content and its threshold values in reflection of soil–plant water status in maize during prolonged drought. *Ecol. Indic.* **2021**, *124*, 107395. [[CrossRef](#)]
11. Finn, M.P.; Lewis, M.; Bosch, D.D.; Giraldo, M.; Yamamoto, K.; Sullivan, D.G.; Kincaid, R.; Luna, R.; Allam, G.K.; Kvien, C.; et al. Remote sensing of soil moisture using airborne hyperspectral data. *GISci. Remote Sens.* **2011**, *48*, 522–540. [[CrossRef](#)]
12. Al-Moustafa, T.; Armitage, R.P.; Danson, F.M. Mapping fuel moisture content in upland vegetation using airborne hyperspectral imagery. *Remote Sens. Environ.* **2012**, *127*, 74–83. [[CrossRef](#)]
13. Ullah, S.; Skidmore, A.K.; Ramoelo, A.; Groen, T.A.; Naeem, M.; Ali, A. Retrieval of leaf water content spanning the visible to thermal infrared spectra. *ISPRS J. Photogramm. Remote Sens.* **2014**, *93*, 56–64. [[CrossRef](#)]
14. Ge, Y.; Atefi, A.; Zhang, H.; Miao, C.; Ramamurthy, R.K.; Sigmon, B.; Yang, J.; Schnable, J.C. High-throughput analysis of leaf physiological and chemical traits with VIS–NIR–SWIR spectroscopy: A case study with a maize diversity panel. *Plant Methods* **2019**, *15*, 66. [[CrossRef](#)] [[PubMed](#)]
15. Zygielbaum, A.I.; Gitelson, A.A.; Arkebauer, T.J.; Rundquist, D.C. Non-destructive detection of water stress and estimation of relative water content in maize. *Geophys. Res. Lett.* **2009**, *36*. [[CrossRef](#)]
16. Ge, Y.; Bai, G.; Stoerger, V.; Schnable, J.C. Temporal dynamics of maize plant growth, water use, and leaf water content using automated high throughput RGB and hyperspectral imaging. *Comput. Electron. Agric.* **2016**, *127*, 625–632. [[CrossRef](#)]
17. Wijewardana, C.; Alsajri, F.A.; Irby, J.T.; Krutz, L.J.; Golden, B.; Henry, W.B.; Gao, W.; Reddy, K.R. Physiological assessment of water deficit in soybean using midday leaf water potential and spectral features. *J. Plant Interact.* **2019**, *14*, 533–543. [[CrossRef](#)]
18. Braga, P.; Crusiol, L.G.T.; Nanni, M.R.; Caranhato, A.L.H.; Fuhrmann, M.B.; Nepomuceno, A.L.; Neumaier, N.; Farias, J.R.B.; Koltun, A.; Gonçalves, L.S.A.; et al. Vegetation indices and NIR-SWIR spectral bands as a phenotyping tool for water status determination in soybean. *Precis. Agric.* **2021**, *22*, 249–266. [[CrossRef](#)]
19. Liu, S.; Peng, Y.; Du, W.; Le, Y.; Li, L. Remote estimation of leaf and canopy water content in winter wheat with different vertical distribution of water-related properties. *Remote Sens.* **2015**, *7*, 4626–4650. [[CrossRef](#)]
20. Liu, L.; Zhang, S.; Zhang, B. Evaluation of hyperspectral indices for retrieval of canopy equivalent water thickness and gravimetric water content. *Int. J. Remote Sens.* **2016**, *37*, 3384–3399. [[CrossRef](#)]
21. Feng, W.; Qi, S.; Heng, Y.; Zhou, Y.; Wu, Y.; Liu, W.; He, L.; Li, X. Canopy vegetation indices from in situ hyperspectral data to assess plant water status of winter wheat under powdery mildew stress. *Front. Plant Sci.* **2017**, *8*, 1219. [[CrossRef](#)]
22. Zhang, J.; Zhang, W.; Xiong, S.; Song, Z.; Tian, W.; Shi, L.; Ma, X. Comparison of new hyperspectral index and machine learning models for prediction of winter wheat leaf water content. *Plant Methods* **2021**, *17*, 34. [[CrossRef](#)] [[PubMed](#)]
23. Zhang, L.; Zhou, Z.; Zhang, G.; Meng, Y.; Chen, B.; Wang, Y. Monitoring the leaf water content and specific leaf weight of cotton (*Gossypium hirsutum* L.) in saline soil using leaf spectral reflectance. *Eur. J. Agron.* **2012**, *41*, 103–117. [[CrossRef](#)]
24. Yi, Q.X.; Bao, A.M.; Wang, Q.; Zhao, J. Estimation of leaf water content in cotton by means of hyperspectral indices. *Comput. Electron. Agric.* **2013**, *90*, 144–151. [[CrossRef](#)]

25. Boshkovski, B.; Doupis, G.; Zapolska, A.; Kalaitzidis, C.; Koubouris, G. Hyperspectral Imagery Detects Water Deficit and Salinity Effects on Photosynthesis and Antioxidant Enzyme Activity of Three Greek Olive Varieties. *Sustainability* **2022**, *14*, 1432. [[CrossRef](#)]
26. Jackson, T.J.; Chen, D.; Cosh, M.; Li, F.; Anderson, M.; Walthall, C.; Doriaswamy, P.; Hunt, E.R. Vegetation water content mapping using Landsat data derived normalized difference water index for corn and soybeans. *Remote Sens. Environ.* **2004**, *92*, 475–482. [[CrossRef](#)]
27. García-Haro, F.J.; Campos-Taberner, M.; Moreno, Á.; Tagesson, H.T.; Camacho, F.; Martínez, B.; Sánchez, S.; Piles, M.; Camps-Valls, G.; Yebra, M.; et al. A global canopy water content product from AVHRR/Metop. *ISPRS J. Photogramm. Remote Sens.* **2020**, *162*, 77–93. [[CrossRef](#)]
28. Cao, Z.; Wang, Q.; Zheng, C. Best hyperspectral indices for tracing leaf water status as determined from leaf dehydration experiments. *Ecol. Indic.* **2015**, *54*, 96–107. [[CrossRef](#)]
29. Ma, S.; Zhou, Y.; Gowda, P.H.; Dong, J.; Zhang, G.; Kakani, V.G.; Wagle, P.; Chen, L.; Flynn, K.C.; Jiang, W. Application of the water-related spectral reflectance indices: A review. *Ecol. Indic.* **2019**, *98*, 68–79. [[CrossRef](#)]
30. Song, L.; Jin, J.; He, J. Effects of Severe Water Stress on Maize Growth Processes in the Field. *Sustainability* **2019**, *11*, 5086. [[CrossRef](#)]
31. Mahlein, A.-K.; Steiner, U.; Dehne, H.-W.; Oerke, E.-C. Spectral signatures of sugar beet leaves for the detection and differentiation of diseases. *Precis. Agric.* **2010**, *11*, 413–431. [[CrossRef](#)]
32. Feng, L.; Zhang, Z.; Ma, Y.; Du, Q.; Williams, P.; Drewry, J.; Luck, B. Alfalfa yield prediction using UAV-based hyperspectral imagery and ensemble learning. *Remote Sens.* **2020**, *12*, 2028. [[CrossRef](#)]
33. ESA—The European Space Agency. Sentinel-2 User Guide. Available online: <https://sentinels.copernicus.eu/web/sentinel/user-guides/sentinel-2-msi> (accessed on 31 March 2021).
34. Wang, F.M.; Huang, J.F.; Tang, Y.L.; Wang, X.Z. New vegetation index and its application in estimating leaf area index of rice. *Rice Sci.* **2007**, *14*, 195–203. [[CrossRef](#)]
35. Gitelson, A.A.; Kaufman, Y.J.; Merzlyak, M.N. Use of a green channel in remote sensing of global vegetation from EOS-MODIS. *Remote Sens. Environ.* **1996**, *58*, 289–298. [[CrossRef](#)]
36. Rouse, J.W.; Haas, R.H.; Schell, J.A.; Deering, D.W. Monitoring vegetation systems in the Great Plains with ERTS. *NASA Spec. Publ.* **1974**, *351*, 309.
37. Gitelson, A.; Merzlyak, M.N. Spectral reflectance changes associated with autumn senescence of *Aesculus hippocastanum* L. and *Acer platanoides* L. leaves. Spectral features and relation to chlorophyll estimation. *J. Plant Physiol.* **1994**, *143*, 286–292. [[CrossRef](#)]
38. Mehdaoui, R.; Anane, M. Exploitation of the red-edge bands of Sentinel 2 to improve the estimation of durum wheat yield in Grombalia region (Northeastern Tunisia). *Int. J. Remote Sens.* **2020**, *41*, 8986–9008. [[CrossRef](#)]
39. Gao, B.C. NDWI—A normalized difference water index for remote sensing of vegetation liquid water from space. *Remote Sens. Environ.* **1996**, *58*, 257–266. [[CrossRef](#)]
40. Hardisky, M.A.; Klemas, V.; Smart, M. The influence of soil salinity, growth form, and leaf moisture on the spectral radiance of spartina alterniflora canopies. *Photogramm. Eng. Remote Sens.* **1993**, *49*, 77–83.
41. Yendrek, C.R.; Tomaz, T.; Montes, C.M.; Cao, Y.; Morse, A.M.; Brown, P.J.; McIntyre, L.M.; Leakey, A.D.B.; Ainsworth, E.A. High-throughput phenotyping of maize leaf physiological and biochemical traits using hyperspectral reflectance. *Plant Physiol.* **2017**, *173*, 614–626. [[CrossRef](#)]
42. Crusiol, L.G.T.; Nanni, M.R.; Furlanetto, R.H.; Sibalidelli, R.N.R.; Cezar, E.; Sun, L.; Foloni, J.S.S.; Mertz-Henning, L.M.; Nepomuceno, A.L.; Neumaier, N.; et al. Yield Prediction in Soybean Crop Grown under Different Levels of Water Availability Using Reflectance Spectroscopy and Partial Least Squares Regression. *Remote Sens.* **2021**, *13*, 977. [[CrossRef](#)]
43. Csajbók, J.; Buday-Bódi, E.; Nagy, A.; Fehér, Z.Z.; Tamás, A.; Virág, I.C.; Bojtor, C.; Forgács, F.; Vad, A.M.; Kutasy, E. Multispectral Analysis of Small Plots Based on Field and Remote Sensing Surveys—A Comparative Evaluation. *Sustainability* **2022**, *14*, 3339. [[CrossRef](#)]
44. Prey, L.; Schmidhalter, U. Simulation of satellite reflectance data using high-frequency ground based hyperspectral canopy measurements for in-season estimation of grain yield and grain nitrogen status in winter wheat. *ISPRS J. Photogramm. Remote Sens.* **2019**, *149*, 176–187. [[CrossRef](#)]
45. Abdulridha, J.; Ampatzidis, Y.; Roberts, P.; Kakarla, S.C. Detecting powdery mildew disease in squash at different stages using UAV-based hyperspectral imaging and artificial intelligence. *Biosyst. Eng.* **2020**, *197*, 135–148. [[CrossRef](#)]
46. Damm, A.; Paul-Limoges, E.; Haghighi, E.; Simmer, C.; Morsdorf, F.; Schneider, F.D.; Tol, C.V.D.; Migliavacca, M.; Rascher, U. Remote sensing of plant-water relations: An overview and future perspectives. *J. Plant Physiol.* **2018**, *227*, 3–19. [[CrossRef](#)]
47. Carter, G.A. Primary and secondary effects of water content on the spectral reflectance of leaves. *Am. J. Bot.* **1991**, *78*, 916–924. [[CrossRef](#)]
48. Sakamoto, T. Incorporating environmental variables into a MODIS-based crop yield estimation method for United States corn and soybeans through the use of a random forest regression algorithm. *ISPRS J. Photogramm. Remote Sens.* **2020**, *160*, 208–228. [[CrossRef](#)]